Published in final edited form as:
Eur J Clin Invest. 2014 March ; 44(3): 325–332. doi:10.1111/eci.12239.

^{18}F-FDG PET/CT as a predictor of hereditary head and neck paragangliomas

Elise M. Blanchet[1], **Sophie Gabriel**[2], **Victoria Martucci**[1], **Nicolas Fakhry**[3], **Clara C. Chen**[4], **Arnaud Deveze**[5], **Corina Millo**[6], **Anne Barlier**[7], **Morgane Pertuit**[7], **Anderson Loundou**[8], **Karel Pacak**[#1], and **David Taïeb**[#2]

[1]Program in Reproductive and Adult Endocrinology, *Eunice Kennedy Shriver* National Institute of Child Health and Human Development, National Institutes of Health, Bethesda, MD, USA.

[2]Department of Nuclear Medicine, La Timone University Hospital, CERIMED, Aix-Marseille University, Marseille, France.

[3]Department of Otorhinolaryngology-Head and Neck Surgery, La Timone University Hospital, Aix-Marseille University, Marseille, France.

[4]Nuclear Medicine Department, Radiology and Imaging Sciences, Warren Magnuson Clinical Center, National Institutes of Health, Bethesda, Maryland, 20892 USA

[5]Department of Otorhinolaryngology-Head and Neck Surgery, North Hospital, Aix-Marseille University, France.

[6]PET Department, Warren Magnuson Clinical Center, National Institutes of Health, Bethesda, Maryland, 20892 USA

[7]Laboratory of Biochemistry and Molecular Biology, Conception Hospital, Aix-Marseille University, Marseille, France.

[8]Department of Public Health, Aix-Marseille University, Marseille, France.

[#] These authors contributed equally to this work.

Abstract

Background—Hereditary head and neck paragangliomas (HNPGLs) account for at least 35% of all HNPGLs, most commonly due to germline mutations in SDHx susceptibility genes. Several studies about sympathetic paragangliomas have shown that ^{18}F-FDG PET/CT was not only able to detect and localize tumors, but also to characterize tumors (^{18}F-FDG uptake being linked to SDHx mutations). However, the data concerning ^{18}FFDG uptake specifically in HNPGLs have not been addressed. The aim of this study was to evaluate the relationship between ^{18}F-FDG uptake and the SDHx mutation status in HNPGL patients.

Methods—^{18}F-FDG PET/CT from sixty HNPGL patients were evaluated. For all lesions, we measured the maximum standardized uptake values (SUVmax), and the uptake ratio defined as HNPGL SUVmax over pulmonary artery trunk SUVmean (SUVratio). Tumor sizes were assessed on radiological studies.

Results—Sixty patients (53.3% with SDHx mutations) were evaluated for a total of 106 HNPGLs. HNPGLs SUVmax and SUVratio were highly dispersed (1.2-30.5 and 1.0-17.0

All correspondence to: Elise Blanchet, Program in Reproductive and Adult Endocrinology, NICHD, NIH Building 10, CRC, 1-East, Room 1-3140, 10 Center Drive, MSC- 1109 Bethesda, Maryland 20892-1109 elise.blanchet@nih.gov.

CONFLICT OF INTEREST STATEMENT
The authors declare that they have no conflict of interest.

respectively). The HNPGL ^{18}F-FDG uptake was significantly higher in SDHx versus sporadic tumors on both univariate and multivariate analysis (p=0.002). We developed two models for calculating the probability of a germline SDHx mutation. The first one, based on a per-lesion analysis, had an accuracy of 75.5%. The second model, based on a per-patient analysis, had an accuracy of 80.0%.

Conclusions—^{18}F-FDG uptake in HNPGL is strongly dependent on patient genotype. Thus, the degree of ^{18}F-FDG uptake in these tumors can be used clinically to help identify patients in whom SDHx mutations should be suspected.

Keywords

PET-CT; head and neck paraganglioma; fluorodeoxyglucose; hereditary cancer; radiopharmaceuticals; genetics

INTRODUCTION

Head and neck paragangliomas (HNPGLs) are neural crest-derived neuroendocrine neoplasms arising from parasympathetic paraganglia. They are distributed from the skull base to the mediastinum with a predilection for the following sites: the jugular foramen (jugular HNPGL), cochlear promontory (tympanic HNPGL), pre-styloid pharyngeal space (vagal HNPGL), and carotid bifurcation (carotid body HNPGL) [1]. HNPGLs were also formerly called glomus tumors. Paragangliomas (PGLs) can develop in the anterior mediastinum; these tumors have the same embryologic origin as HNPGLs and also develop from parasympathetic paraganglia. Thus, PGL of the anterior mediastinum can be considered the same entity as HNPGLs.

HNPGLs are more often hereditary than their sympathetic counterparts [2-5]. Of all the known PGL susceptibility genes, mutations in SDHD are currently the leading cause of HNPGLs, followed by SDHB and SDHC mutations [2, 4-6]. HNPGLs also exhibit some unique features, such as the absence of catecholamine secretion in most cases, a low rate of malignancy, and different phenotypes on molecular imaging [7]. Thus, HNPGLs are an entity distinct from sympathetic PGLs (symp-PGLs) and, as such, deserve specific studies.

In recent years, several studies have shown that besides detecting tumors, ^{18}F FDG PET/CT could characterize them by providing an indication as to possible genotype. An extensive study found that tumor ^{18}F-FDG uptake was higher in patients with SDHx germline mutations [8]. The discovery of such a metabolic imaging pattern may become crucial to further elucidating the pathogenesis of these tumors and help improve prognosis prediction, treatment selection, and therapeutic response evaluation. However, the data concerning ^{18}F-FDG uptake in HNPGL have not been specifically addressed so far. It is notable that ^{18}F-FDOPA PET/CT is a highly sensitive and specific tracer for localizing these tumors [9-11], but as the uptake of this radiotracer is almost always very intense regardless of genotype, this fails to provide information regarding the genotype [11]. Furthermore, ^{18}F-FDOPA is not routinely available at most imaging centers worldwide. HNPGLs can be detected by ^{18}F-FDG PET/CT with good sensitivities (77-85%) [8, 9], but unlike ^{18}F-FDOPA, the uptake is not constantly high; there is a wide range of uptake values among patients with HNPGL. We therefore hypothesized that this variability would be closely related to patient genotypes.

The aim of the present study was to evaluate the relationship between tumor ^{18}F-FDG uptake and patient genotypes in a large cohort of patients evaluated at two academic endocrine tumor centers.

MATERIALS AND METHODS

Patients

^{18}F-FDG PET/CT studies performed for HNPGL imaging in two academic endocrine tumor centers (La Timone University Hospital and the National Institutes of Health (NIH)) between 2008 and 2013 were reviewed. Only patients who fulfilled the following criteria were retrospectively included:

1. at least one HNPGL at the time of PET/CT study,
2. genetic screening was performed for SDHB, SDHC, SDHD, VHL, SDHAF2, TMEM127, and MAX.

Patients had at least one HNPGL identified on the basis of conventional imaging (CT and MRI) at the time of the PET/CT study. The indication for ^{18}F-FDG PET/CT was to determine whether additional tumors were present and to diagnose malignant tumors (a definition which is strictly based on the finding of metastatic disease). No patient underwent imaging because of suspicion of locoregional recurrent disease.

We obtained written informed consent from all patients for PET scanning as well as DNA testing according to protocols approved by local ethics committees.

^{18}F-FDG PET scanning

All patients fasted for a minimum of 6h prior to intravenous injection of ^{18}F-FDG (4 to 5 MBq/kg), and blood glucose levels were measured just before injection to ensure a value below 200 mg/dL. Scanning began 60 min (65 min +/−10 min) following tracer injection. The PET/CT acquisitions were performed on a Discovery ST PET/CT scanner (GE Healthcare) or on a Biograph-128 mCT PET/CT scanner (Siemens Medical Solutions). A non-diagnostic CT from the head to the thighs was performed without contrast. Immediately after the CT scan, a PET scan covering the same field of view was obtained in 3D mode with an acquisition time of 3 min per bed position. PET image datasets were reconstructed iteratively (OSEM algorithm) on a 256 × 256 matrix using CT data for attenuation correction. Co-registered images were displayed with 3D fused navigation along the axial, coronal, and sagittal planes and maximum intensity projection (MIP) rendering.

Image interpretation and quantitative measurements

At each participating institution, the ^{18}F-FDG PET scans were reviewed by two experienced nuclear medicine physicians blinded to the reports of other functional and anatomic imaging studies. The ^{18}F-FDG uptake was assessed for each lesion, visually and quantitatively. Visually, ^{18}F-FDG uptake was considered pathologic if there was focal uptake more intense than surrounding background in areas recognized as sites of parasympathetic HNPGL development [1]. Lesions were classified as tympanic, jugular, carotid, and vagal (cervical and mediastinal) HNPGLs.

For quantitative assessment, maximum standardized uptake values (HNPGL-SUVmax) were calculated using the following formula: the SUV equaled the decay-corrected tracer tissue concentration (in Bq/g) of the injected dose (in Bq) normalized by the patient's body weight (in g). The SUVmax were measured on attenuation-corrected PET images. Mean SUV (SUVmean) was also measured in the pulmonary artery trunk (PAT) on 2-dimensional regions of interest covering two thirds of the pulmonary artery diameter, in order to evaluate an uptake ratio defined as HNPGL-SUVmax over PATSUVmean. We calculated this tumor-to-blood pool-background ratio because two different scanners were used (La Timone / NIH).

The three anatomic dimensions of each lesion were measured on the latest CT or MRI, and the tumor volume was calculated using the ellipse volume formula (volume = length × width × height × π/6). The time interval between CT/MRI and PET/CT imaging was 30 days at maximum.

Standard of truth

Pathological analysis of the tumor was considered the gold standard for the diagnosis of an HNPGL. In cases where no surgical resection was performed, the diagnosis of HNPGL was made if the lesion was located in a classical anatomic site for HNPGL and confirmed by a second imaging procedure using a specific tracer (^{18}F-FDOPA, OctreoScan).

In the present study, 30 (/57) and 34 (/49) tumors were surgically removed at NIH and Timone, respectively. Among the non-surgically removed tumors, 40 were confirmed with ^{18}F-FDOPA PET/CT and two with Octreoscan.

Statistical analysis

Statistical analysis was performed using IBM SPSS Statistics version 20 (IBM SPSS Inc., Chicago, IL, USA) and Medcalc version 12.7. Continuous variables are expressed as means ± standard deviation or as a median with a range (min, max), and categorical variables are expressed as count and percentages. Comparisons of mean values between two groups were performed using a student t-test or Mann-Whitney U. Comparisons of percentages were performed using a Chi-Square test or Fisher's exact test, as appropriate. Multivariate analysis was performed using a logistic regression model to estimate the risk factors for an SDHx mutation. Calibration of the logistic model was assessed using the Hosmer-Lemeshow goodness-of-fit test to evaluate the discrepancy between observed and expected values. Odds-ratios were expressed with 95% confidence intervals. The area under the receiver operating characteristic (ROC) curve was used to define a cut-off value using predicted values, and a formula was proposed. A classification table was used to evaluate the predictive accuracy of the logistic regression model and the discriminative ability of mutation status was quantified by the measures of diagnostic accuracy. For all tests, a two-sided p-value less than 0.05 was considered statistically significant.

RESULTS

Patients and clinical characteristics

A total of 62 patients with HNPGL were evaluated with ^{18}F-FDG PET/CT. Of them, 60 patients (21 men, 39 women; age range 12–84 years) fulfilled all criteria and were retrospectively included in the present study. Two patients were not included because genetic testing had not been done (one patient died and one patient declined the genetic testing). HNPGLs (106 tumors) were distributed as follows: 1 tympanic, 27 jugular, 50 carotid body, 26 vagal (cervical or mediastinal), and 2 in other locations (nasosinusal, laryngeal). Five patients were found to have malignant tumors (4 distant metastases, 1 locoregional recurrence with metastatic lymph nodes). Twenty-three patients had multiple primary parasympathetic HNPGLs.

Thirty-two patients (53.3%) had a germline mutation in one of the SDHx genes: 11 SDHB, 2 SDHC, 19 SDHD. No mutations were found in the SDHAF2, VHL, TMEM127, or MAX genes. Therefore, all the patients without SDHx germline mutations were apparently sporadic in our study. SDHx patients were younger (45.7 ± 15.8 vs 62.6 ± 15.9, $p<0.001$) and more frequently male (15/21 vs 17/39, $p=0.04$) than sporadic patients. Multiple primary HNPGLs were detected in 4/28 sporadic (as shown in Figure 1), 3/11 SDHB, 0/2 SDHC, and 16/19 SDHD patients. Concomitant sympathetic abdominal PGLs (pheochromocytomas

or extra-adrenal PGLs) were present in 8 SDHD patients. SDHx-related PGLs were at a higher risk for multifocal tumors than their sporadic counterparts ($p<0.001$).

^{18}F-FDG PET/CT detection rates

On visual analysis, 90.5% (96/106) of HNPGL lesions were detected with ^{18}F-FDG PET/CT. Of the 10 ^{18}F-FDG negative tumors, 7/73 were from SDHx patients and 3/33 were from sporadic patients. The per-lesion detection rate was not statistically different in SDHx-related lesions versus non-SDHx-related lesions (90.9% in sporadic versus 90.4% in SDHx). The overall per-patient detection rate was 86.6% (52/60). The per-patient detection rate in SDHx-related lesions was 84.4% (27/32) versus 89.3% in non-SDHx-related lesions (25/28). All 7 missed SDHx-related lesions had a tumor volume of <500 mm^3 and largest diameter of <10 mm. The 3 missed sporadic cases had larger tumor diameters (63, 22, and 36 mm) and volumes (2700, 31600, and 8200 mm^3).

^{18}F-FDG uptake in relation to patient genotype

On univariate analysis, HNPGL-SUVmax and SUV ratio (HNPGL-SUVmax/PAT-SUVmean) were statistically different between tumors from SDHx versus non-SDHx patients: HNPGL-SUVmax was 3.4 (1.8-30.5) in tumors from non-SDHx patients versus 7.8 (1.2-28.3) in tumors from SDHx patients, and SUV ratio was 2.3 (1.0-17.0) in tumors from non-SDHx patients versus 5.6 (1.0-16.2) in tumors from SDHx patients. On multivariate analysis, a high SUV ratio (HNPGL-SUVmax/PA-SUVmean) was significantly associated with the presence of a germline SDHx mutation, independent of the tumor size (Table 1).

Tumor SUVmax and ratio did not differ significantly between patients from the two institutions: for SDHx tumors, SUVmax was 8.0 (1.2-28.1) at NIH and 7.3 (1.2-28.3) at Timone (Mann-Whitney U, $p=0.625$), and SUV ratio was 5.7 (1-16.2) at NIH and 5.5 (1.2-15.2) at Timone ($p=0.341$); for sporadic cases, ratio values did not statistically differ between the two institutions ($p=0.270$). PAT SUVmean did not differ significantly between the two institutions (1.3 (1.0-1.8) at NIH and 1.5 (0.9-2.6) at Timone, $p= 0.137$).

^{18}F-FDG uptake as a predictor of a germline SDHx mutation: lesion-based model

Taking into account the wide inter- and intra-patient variability in tumor size and the major influence of tumor size on uptake values through partial volume effect, we therefore adapted our model to these parameters. The following formula (Equation 1) was generated by the logistic regression model for calculating the probability (P) of a germline SDHx mutation based on the SUVmax ratio (R) and the largest tumor diameter (D) in mm:

$$P=\frac{\exp\left(1.146+0.240*R-0.062*D\right)}{1+\exp\left(1.146+0.240*R-0.062*D\right)} \quad \text{(Equation 1)}$$

Its curve is displayed in Figure 2. As shown in the figure, tumors with very high SUV ratios had a high probability of belonging to an SDHx patient, regardless of the tumor size. By contrast, for tumors with low SUV ratios, the probability of belonging to an SDHx-mutated patient was highly dependent on tumor size. According to this lesion-based model, an ROC curve was built, and the optimal threshold point was 65.97 (Figure 3A). With this threshold point, sensitivity (Se), specificity (Sp), positive predictive value (PPV), negative predictive value (NPV), and accuracy were 80.8%, 63.6%, 83.1%, 60.0%, and 75.5%.

^{18}F-FDG uptake as a predictor of a germline SDHx mutation: patient-based model

The model was also applied to individual subjects and refined by the inclusion of their age in years (A), presence of multifocality (M, 1=no or 2=yes), largest tumor diameter (D in

mm), and SUV ratio (R) of the most-avid tumor. The following formula (Equation 2) was generated for calculating the probability (P) of an SDHx mutation:

$$P=\frac{\exp\left(3.2+0.142*R-0.049*D+1.6*M-0.06*A\right)}{1+\exp\left(3.2+0.142*R-0.049*D+1.6*M-0.06*A\right)} \quad \text{(Equation 2)}$$

Using this patient-based model, a second ROC curve was built, and the optimal threshold point was 74.22 (Figure 3B). With this threshold point, Se, Sp, PPV, NPV, and accuracy were 62.5%, 100%, 100%, 70.0%, and 80.0%.

DISCUSSION

The present study describes the detection rate and the uptake of ^{18}F-FDG PET in a large cohort of HNPGLs with and without associated genetic mutations. Overall, the lesion-based detection rate was 90.5% (with no difference between SDHx-mutated and sporadic tumors). Interestingly, ^{18}F-FDG uptake was higher in SDHx-mutated compared to apparently sporadic tumors despite their similar detection rate. Thus, we developed two models to predict SDHx mutation by using ^{18}F-FDG uptake, in combination with the largest tumor diameters (lesion-based model) or other clinical predictor variables (patient-based model).

PET imaging has gained major recognition in the evaluation of patients with HNPGLs. ^{18}F-FDOPA PET/CT has proved to be a highly sensitive imaging modality for localizing HNPGLs, with a high tumor-to-background contrast, regardless of the genotype [9-12]. PET imaging using ^{68}Ga-DOTA-somatostatin analogs has also demonstrated promising results, especially in the evaluation of metastatic pheochromocytomas (PHEOs) and PGLs [13]. One study compared ^{68}Ga-DOTANOC and ^{18}F-FDOPA PET/CT in patients with PHEO/PGLs. However, in this study, no information was given regarding patient genotypes [14]. As recommended by the EANM guidelines, ^{18}F-FDOPA-PET/CT or ^{68}Ga-DOTA-somatostatin analog PET/CT should be used as the first-line functional imaging procedures for HNPGL patients [7]. However, these tracers are not routinely available at most imaging centers worldwide. In contrast, ^{18}F-FDG PET/CT is commonly available. Additionally, in contrast to ^{18}F-FDOPA, ^{18}FFDG PET/CT also enables characterization of HNPGLs. Although we are still far from being able to provide an *"in vivo"* histology by imaging, we feel that nuclear imaging may help in characterizing HNPGLs and predict their behavior. This would be of great relevance in the management of patients with HNPGLs.

In this study, we found that increased ^{18}F-FDG uptake (expressed as SUVmax or SUV ratio) was associated with the presence of SDHx mutations. In symp-PGLs, Timmers et al. [8] found a similar pattern, in which the SUVmax in non-metastatic PGLs for hereditary tumors related to the SDHB, SDHD, and VHL mutations was statistically significantly higher (14.3 ± 6.3, $p<0.05$) than for hereditary tumors related to MEN2 and NF1 mutations (3.1 ± 1.5) and sporadic tumors (7.0 ± 6.0 for non-epinephrine–producing tumors and 3.8 ± 1.6 for epinephrine-producing tumors). It is well accepted that ^{18}F-FDG uptake and retention is governed by the expression of glucose transporters (GLUTs) and expression and activity of hexokinase-2 (HK2) [15]. Upregulation of GLUTs and HK2 mRNA are found in SDHx-related PGLs [16]. This could explain the intense ^{18}F-FDG uptake in SDHx-related PGLs/HNPGLs.

Our results emphasize the importance of providing quantitative parameters in nuclear medicine reports as meaningful insights into tumor biology. The provided data could enable us to calculate a risk probability for SDHx mutation and thus guide genetic testing. These models are easily used by putting the SUV ratio and the largest tumor diameter into Equation 1, or, alternatively, the patient's age, the presence of multifocality, the largest

tumor diameter, and the most-avid tumor SUV ratio in Equation 2. As an example of using our models, a patient with a 40 mm (largest diameter) single HNPGL has a 75% probability of having an SDHx mutation if the SUV ratio is equal to 10. The same probability is observed in a patient with a 20 mm HNPGL and a ratio of 5. The use of clinical predictors (age, multifocality) also increases the performance of the model.

We acknowledge the limits of using the SUVmax as a biomarker for tumor uptake: SUVmax is affected by noise, and assessment of a single pixel may not be representative of the overall tumor uptake [17]. HNPGL SUVmean was not assessed in the present study. Because of physiological ^{18}F-FDG uptake in the head and neck area (in brain and lymphatic tissues), automated delineation using a fixed threshold was not possible, and manual delineation of the regions of interest (ROIs) do not allow reproducible measurement of SUVmean. SUVmax is less dependent on ROI delineation than SUVmean. Furthermore, SUVmax is the parameter least affected by partial volume effect, which becomes a critical problem when tumors are smaller than two centimeters [17]. Furthermore, in contrast to PHEO uptake, we have observed that ^{18}F-FDG uptake is often relatively homogeneous in HNPGLs. Use of SUVmax could also be criticized from a biological standpoint. SUV assumes that the unmetabolized component of a radiopharmaceutical (e.g., in blood within a tumor, in intercellular spaces, and within tumor cells themselves) is negligible. This assumption may be detrimental in the understanding of the tumor biology of PGLs, since these tumors frequently show a high vascular volume fraction and a low metabolization rate. Therefore, unmetabolized ^{18}F-FDG may be far from negligible in HNPGLs, even when evaluating delayed images. This aspect remains to be further evaluated. Quantitative methods (Patlak analysis, SKA-S) have been developed to overcome the shortcomings of SUV. However, these methods suffer from practical constraints. Despite its imperfections mainly related to noise, SUVmax remains the most widely used parameter. In the current study we used the pulmonary artery activity as an equivalent for venous blood activity, in order to obtain a target-to-background ratio. In our opinion, this reference area is reliable. Other studies have used the liver in characterizing the background uptake, but its activity could be influenced by many factors [18].

A possibility that cannot be excluded is that somatic mutations could also occur and influence the tumor metabolic profile. Even though this challenges the validity and amplifies the complexity required by our model, the proposed approach in this study could help to improve knowledge in pathogenesis and tumor biology of HNPGL.

CONCLUSION

Our results suggest that ^{18}F-FDG in HNPGLs, in addition to its qualitative information (detection and localization of tumor), provides quantitative information relevant for understanding the tumor biology and predicting the patient's genotype. This is valid for tumors larger than 1 cm (for smaller tumors SUVs appear unreliable). The present approach is encouraging in the context of hereditary HNPGL. Further studies are needed to validate and refine these models in larger patient cohorts and at other centers with different patient populations.

REFERENCES

1. Lee KY, Oh YW, Noh HJ, Lee YJ, Yong HS, Kang EY, et al. Extraadrenal paragangliomas of the body: imaging features. American Journal of Roentgenology. 2006; 187:492–504. [PubMed: 16861555]
2. Neumann HP, Erlic Z, Boedeker CC, Rybicki LA, Robledo M, Hermsen M, et al. Clinical predictors for germline mutations in head and neck paraganglioma patients: cost reduction strategy in genetic diagnostic process as fall-out. Cancer Res. 2009; 69:3650–6. [PubMed: 19351833]

3. Mannelli M, Castellano M, Schiavi F, Filetti S, Giacche M, Mori L, et al. Clinically guided genetic screening in a large cohort of italian patients with pheochromocytomas and/or functional or nonfunctional paragangliomas. J Clin Endocrinol Metab. 2009; 94:1541–7. [PubMed: 19223516]
4. Burnichon N, Rohmer V, Amar L, Herman P, Leboulleux S, Darrouzet V, et al. The succinate dehydrogenase genetic testing in a large prospective series of patients with paragangliomas. J Clin Endocrinol Metab. 2009; 94:2817–27. [PubMed: 19454582]
5. Jafri M, Whitworth J, Rattenberry E, Vialard L, Kilby G, Kumar AV, et al. Evaluation of SDHB, SDHD and VHL gene susceptibility testing in the assessment of individuals with non-syndromic phaeochromocytoma, paraganglioma and head and neck paraganglioma. Clinical endocrinology. 2013; 78:898–906. [PubMed: 23072324]
6. Bayley JP, Kunst HP, Cascon A, Sampietro ML, Gaal J, Korpershoek E, et al. SDHAF2 mutations in familial and sporadic paraganglioma and phaeochromocytoma. Lancet Oncol. 2010; 11:366–72. [PubMed: 20071235]
7. Taieb D, Timmers HJ, Hindie E, Guillet BA, Neumann HP, Walz MK, et al. EANM 2012 guidelines for radionuclide imaging of phaeochromocytoma and paraganglioma. Eur J Nucl Med Mol Imaging. 2012; 39:1977–95. [PubMed: 22926712]
8. Timmers HJ, Chen CC, Carrasquillo JA, Whatley M, Ling A, Eisenhofer G, et al. Staging and functional characterization of pheochromocytoma and paraganglioma by 18F-fluorodeoxyglucose (18F-FDG) positron emission tomography. J Natl Cancer Inst. 2012; 104:700–8. [PubMed: 22517990]
9. King KS, Chen CC, Alexopoulos DK, Whatley MA, Reynolds JC, Patronas N, et al. Functional imaging of SDHx-related head and neck paragangliomas: comparison of 18F-fluorodihydroxyphenylalanine, 18F-fluorodopamine, 18F-fluoro-2-deoxy-D-glucose PET, 123I-metaiodobenzylguanidine scintigraphy, and 111In-pentetreotide scintigraphy. J Clin Endocrinol Metab. 2011; 96:2779–85. [PubMed: 21752889]
10. Treglia G, Cocciolillo F, de Waure C, Di Nardo F, Gualano MR, Castaldi P, et al. Diagnostic performance of 18F-dihydroxyphenylalanine positron emission tomography in patients with paraganglioma: a meta-analysis. Eur J Nucl Med Mol Imaging. 2012; 39:1144–53. [PubMed: 22358431]
11. Gabriel S, Blanchet EM, Sebag F, Chen CC, Fakhry N, Deveze A, et al. Functional characterization of nonmetastatic paraganglioma and pheochromocytoma by (18) F-FDOPA PET: focus on missed lesions. Clinical endocrinology. 2013; 79:170–7. [PubMed: 23230826]
12. Taieb D, Varoquaux A, Chen CC, Pacak K. Current and future trends in the anatomical and functional imaging of head and neck paragangliomas. Semin Nucl Med. 2013; 43:462–73. [PubMed: 24094713]
13. Sharma P, Thakar A, Suman Kc S, Dhull VS, Singh H, Naswa N, et al. 68Ga- DOTANOC PET/CT for Baseline Evaluation of Patients with Head and Neck Paraganglioma. Journal of nuclear medicine : official publication, Society of Nuclear Medicine. 2013; 54:841–7.
14. Kroiss A, Putzer D, Frech A, Decristoforo C, Uprimny C, Gasser RW, et al. A retrospective comparison between (68)Ga-DOTA-TOC PET/CT and (18)F-DOPA PET/CT in patients with extra-adrenal paraganglioma. Eur J Nucl Med Mol Imaging. 2013; 40:1800–8. [PubMed: 24072345]
15. Mathupala SP, Ko YH, Pedersen PL. Hexokinase-2 bound to mitochondria: cancer's stygian link to the “Warburg Effect” and a pivotal target for effective therapy. Seminars in cancer biology. 2009; 19:17–24. [PubMed: 19101634]
16. Favier J, Briere JJ, Burnichon N, Riviere J, Vescovo L, Benit P, et al. The Warburg effect is genetically determined in inherited pheochromocytomas. PLoS One. 2009; 4:e7094. [PubMed: 19763184]
17. Soret M, Bacharach SL, Buvat I. Partial-volume effect in PET tumor imaging. Journal of nuclear medicine : official publication, Society of Nuclear Medicine. 2007; 48:932–45.
18. Groheux D, Delord M, Rubello D, Colletti PM, Nguyen ML, Hindie E. Variation of liver SUV on (18)FDG-PET/CT studies in women with breast cancer. Clinical nuclear medicine. 2013; 38:422–5. [PubMed: 23510894]

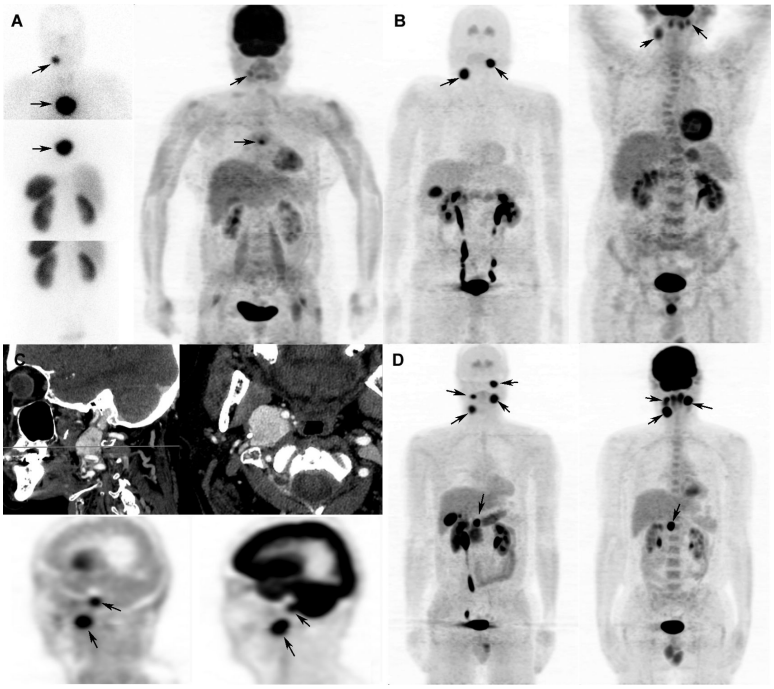

Figure 1. Examples of patients with multifocal tumors

A. Sporadic patient with a right carotid HNPGL and a mediastinal parasympathetic PGL. On the left side, somatostatin receptor scintigrapy (SRS) shows both tumors. On the right side, ^{18}F-FDG PET/CT (maximum intensity projection - MIP) is displayed: the right carotid HNPGL is very weakly hypermetabolic compared to the background (SUV ratio of 2.1); the mediastinal parasympathetic PGL is partially mildly hyper-metabolic (SUV ratio of 2.3).

B. Sporadic patient with a right carotid HNPGL and a left vagal HNPGL. On the left, ^{18}F-FDOPA PET/CT (MIP) shows high tumor uptake. On the right, ^{18}FFDG PET/CT (MIP) is displayed: the right carotid HNPGL and the left vagal HNPGL are both moderately hyper-metabolic (SUV ratios of 3.9 and 3.5, respectively).

C. Sporadic patient with a right jugular HNPGL and a right vagal HNPGL. Upper images display contrast-enhanced CT images (sagittal and axial). On the lower left, ^{18}F-FDOPA PET/CT (sagittal CT attenuation-corrected PET image) shows both HNPGLs with high ^{18}F-FDOPA uptake. On the right, ^{18}F-FDG PET/CT (sagittal CT attenuation-corrected PET image) is displayed: the right jugular HNPGL is moderately hyper-metabolic (SUV ratio of 3.3); the right vagal HNPGL is intensely hyper-metabolic (SUV ratio of 12.4).

D. **SDHD patient with multiple HNPGLs**. On the left, ^{18}F-FDOPA PET/CT (MIP) shows four HNPGLs with high ^{18}F-FDOPA uptake. On the right, ^{18}F-FDG PET/CT (MIP) is displayed: the left jugular moderately hyper-metabolic (SUV ratio of 3.7) but cannot be separated from brain on the image shown, and the left vagal, right vagal, and right carotid body HNPGLs are all intensely hyper-metabolic (SUV ratios of 10.6, 5.4, and 15.2, respectively).

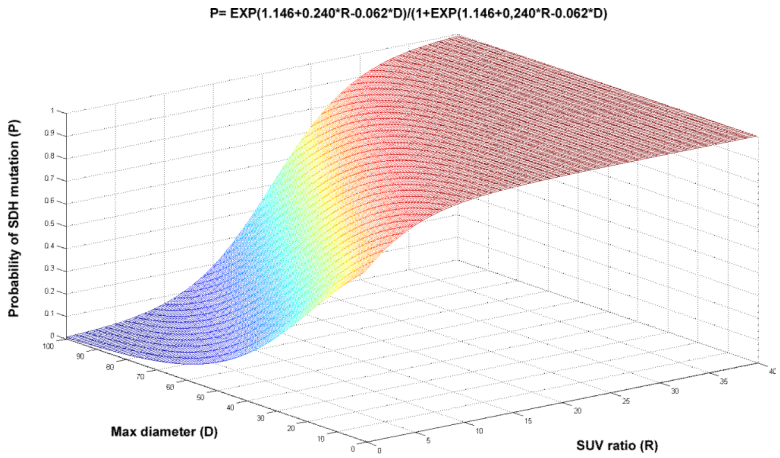

Figure 2. Graphical representation of the probabilities of tumors being related to a germline SDHx mutation

(using Equation 1).

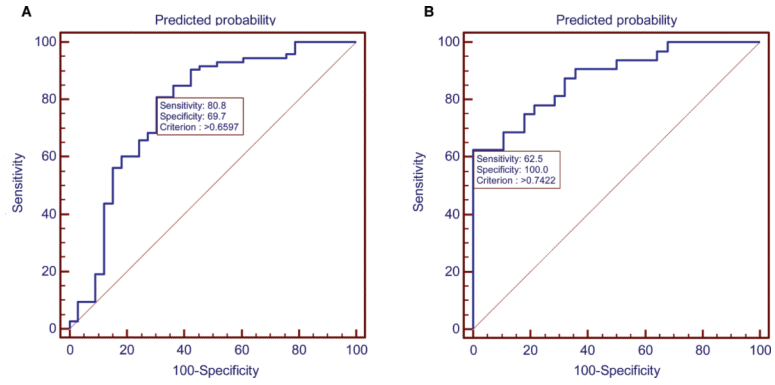

Figure 3. ROC curves

A. Lesion-based model

B. Patient-based model

Table 1

Factors influencing SDHx mutation status. HNPGL-SUVmax, SUV ratio (HNPGL-SUVmax over pulmonary artery trunk SUVmean), largest tumor diameter in mm, and tumor volume in mm^3 are presented as averages (range).

	Univariate			Multivariate		
	SDH− N=33	**SDH+ N=73**	**P**	**OR**	**95% CI**	**P**
Tumor location						
Tympanic	*1*	*0*				
Jugular	*9*	*18*				
Carotid	*16*	*34*	0.661			
Vagal (cervical or mediastinal)	*6*	*20*				
other	*1*	*1*				
HNPGL-SUVmax	3.4 (1.8-30.5)	7.8 (1.2-28.3)	**<0.001**			
SUV ratio	2.3 (1.0-17.0)	5.6 (1.0-16.2)	**<0.001**	1.3	1.1-1.5	**0.002**
Largest tumor diameter in mm	27 (8-63)	21 (6-60)	**0.009**	0.9	0.91-0.98	**0.001**
Tumor volume in mm^3	4717 (147174)	2059 (469357)	**0.009**			